Spherical Mean Diffusion-Weighted MRI Reveals Peripheral Axonal Pathology Following Trauma

Kelvin Chen[1, 2]; Thammathida Ketsiri, Ph.D.[1]; Richard D. Dortch, Ph.D.[1]

[1]Department of Translational Neuroscience, Barrow Neurological Institute, Phoenix, AZ, USA
[2]University of Virginia, Charlottesville, VA, USA

ABSTRACT

The spherical mean technique (SMT) is a multi-compartmental diffusion MRI model of white matter that yields indices of tissue microstructure specific to the extra- and intra-axonal compartments in the nervous system, which may reveal evidence of nerve re/degeneration in cases of traumatic peripheral nerve injury (TPNI). Of note, the current clinical management of TPNI is complicated by challenges in assessing nerve injury severity and monitoring the success of post-operative nerve regeneration, thereby delaying clinical decision-making. Here we present a preclinical validation of SMT to estimate axonal volume fraction (V_{ax}) and axonal diffusivity (Dax) from computer simulations based on pathologically realistic tissue geometries from light microscopy data. Following model validation and optimization, simulation-based SMT-derived estimates displayed strong agreements with experimental data from both histology and diffusion MRI. SMT-based diffusion biomarkers may thus offer improved pathological specificity and sensitivity to nerve re/degeneration relative to conventional MRI methods (e.g., DTI, DKI, MRN), which effectively moves SMT toward clinical trial readiness, where it will be tested for its ability to detect failed nerve repairs earlier than current diagnostic methods and predict surgical outcomes.

INTRODUCTION

Peripheral nerves characteristically undergo axonal loss, demyelination, edema, and unorganized regeneration following trauma and/or surgical nerve repair[1], resulting in microstructural alterations that can be detected with diffusion MRI.

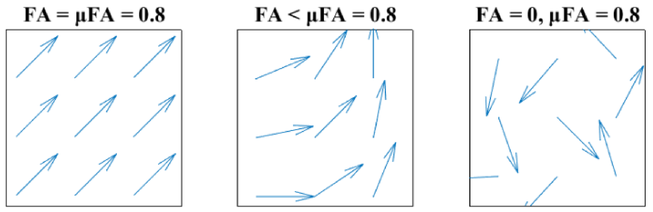

Figure 1. The degree of anisotropy reflects the directional architecture of water protons (denoted by the arrows) in a diffusion process. Global measures (e.g. fractional anisotropy, FA) are confounded by complex, arbitrary axon orientation distributions (single orientation, left; fiber dispersion, middle; uniform distribution, right) resulting from fiber crossings, orientation dispersion (e.g. neuroma), and axon undulations. These effects are eliminated in SMT, however, for it is an orientation-invariant method by which diffusion signals are averaged across all gradient directions, resulting in measures of local microscopic FA (μFA).[2, 3]

METHODS

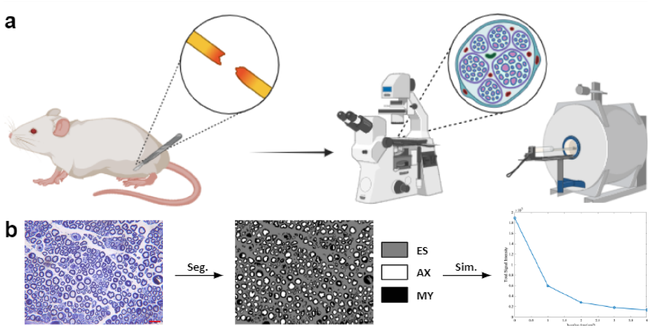

Figure 2. Distal sciatic nerves were harvested from rat models of TPNI and categorized by injury type (sham, crush, cut/repair) and post-operative time point (1, 2, 4, 12 weeks) (a). Toluidine blue-stained histology images (scale bar: 20 μm) from light microscopy and MRI were semantically segmented into three compartments (extra-axonal, ES; intra-axonal, AX; myelin/debris, MY) followed by simulating the diffusion signals via the finite difference method with SMT fitting (b).

Generalized SMT Model Assumptions[3]:

- Myelin signals are excluded due to a rapid T_2 relaxation while the T_2s of extra- and intra-axonal spaces are homogeneous.
- Axial diffusivities along the axonal fibers are the same wherein $D_{ax} = D_{\parallel}^{ext} = D_{\parallel}^{int}$ due to the lack of restriction per axon.
- The first-order tortuosity limit is true such that $D_{\perp}^{ext} = (1-V_{ax})D_{ax}$ and $D_{\perp}^{int} \approx 0$ due to minuscule axon diameters (1–2 μm).

SMT Modeling. The spherical mean diffusion signal $\bar{S}$ was derived from isolated mean extra- and intra-axonal signals to approximate the parameters $V_{ax} \in [0, 1]$ and $D_{ax} \in [0, D_{ax}^{free}]$, where $D_{ax}^{free} \approx 1.88$ μm^2/ms at 17 °C for ex vivo rodent models.[2]

$$\underbrace{h_b(g,\omega \mid V_{ax}, D_{ax}) = V_{ax}h_b^{int}(g,\omega) + (1-V_{ax})h_b^{ext}(g,\omega)}_{\text{Multi-compartment microscopic diffusion model}} \xrightarrow{\text{SMT}} \underbrace{\bar{S} = V_{ax}\bar{S}_{int} + (1-V_{ax})\bar{S}_{ext}}_{\text{Mean diffusion signal model}} \quad (1)$$

For comparison, more conventional attenuated diffusion signals due to Gaussian and non-Gaussian water diffusion were quantified by ADC and kurtosis, respectively.[4]

$$\underbrace{S(b) = S_0 \exp(-b\bar{D})}_{\text{Stejskal-Tanner equation}} \xrightarrow{\text{Cumulant expansion}} \underbrace{S(b) = S_0 \exp\left(-b\bar{D} + \frac{1}{6}b^2\bar{D}^2\bar{K} + O(b^3)\right)}_{\text{Standard DKI signal representation}} \quad (2)$$

Diffusion MRI Signal Simulation & Analysis. Simulations were performed in 3D geometry (stacked 2D sections) with restricted diffusion in silico in MATLAB with the MATI (Microstructural Analysis of Tissues by Imaging) package. Results were compared against their corresponding ground truth to test model assumptions and the precision and accuracy of optimized SMT parameters.

RESULTS & DISCUSSION

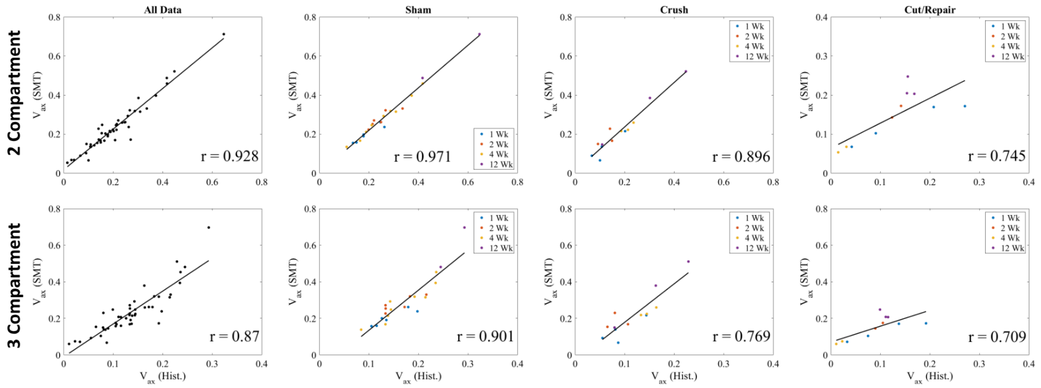

Figure 3. Correlation between SMT- and histology-derived V_{ax} was shown to be significantly linear for each injury type across all post-operative time points in the Pearson plots, notably in the two-compartment model where signal contributions from myelin were excluded.

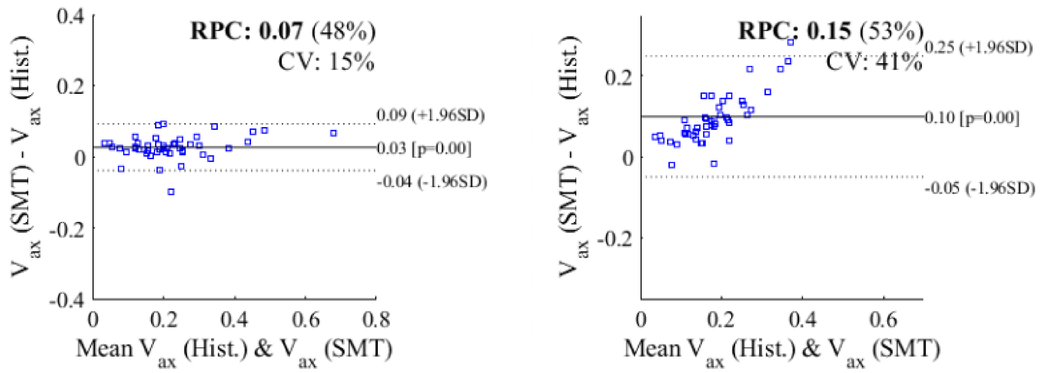

Figure 4. In comparison to the three-compartment model (right), a stronger agreement was observed in the two-compartment model (left) with higher repeatability and lower variability relative to the mean as shown in the Bland-Altman plots.

Type	Harvest	V_{ax} (Histology)	V_{ax} (SMT)		
			$b \in [0, 0.8, 1.6, 2.4, 3.2]$	$b \in [0, 1, 2, 3, 4]$	$b \in [0, 1.2, 2.4, 3.6, 4.8]$
Sham	1 wk	0.246	0.275	0.261	0.246
Crush	1 wk	0.202	0.225	0.215	0.205
Cut/Repair	1 wk	0.091	0.109	0.102	0.096

Type	Harvest	MD (μm^2/ms)	D_{ax} (SMT)		
			$b \in [0, 0.8, 1.6, 2.4, 3.2]$	$b \in [0, 1, 2, 3, 4]$	$b \in [0, 1.2, 2.4, 3.6, 4.8]$
Sham	1 wk	0.842	1.788	1.726	1.663
Crush	1 wk	0.763	1.779	1.736	1.690
Cut/Repair	1 wk	0.950	1.772	1.739	1.704

(a) Impact of varied sets of b-values on V_{ax} (top) and D_{ax} (bottom) approximations in the SMT-based diffusion model; errors were observed to have decreased with an increase in b-values.

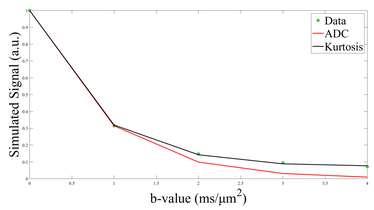

Figure 5. Signal decay as a function of a set of b-values due to Gaussian and non-Gaussian diffusivities.

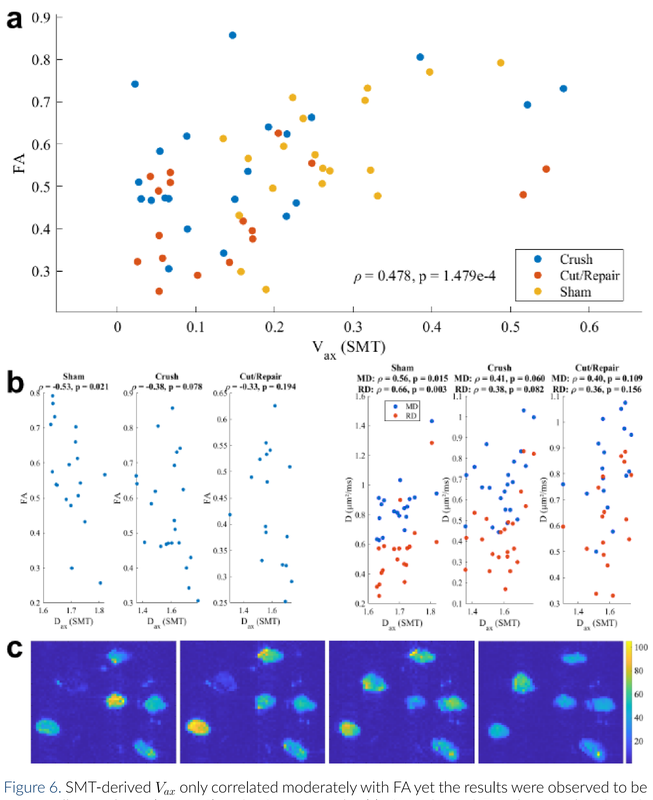

Figure 6. SMT-derived V_{ax} only correlated moderately with FA yet the results were observed to be statistically significant ($p \leq 0.05$) in the Spearman plot (a). SMT-derived D_{ax} also correlated moderately with FA and measures of diffusivity (MD, RD), but no statistical significance was observed in the said relationship (b). Note the reduced FA and elevated diffusivities in the representative distal slices of DTI/DKI parameter maps, which are indicative of partial nerve re/degeneration (c).

CONCLUSION

SMT yielded tissue-specific measures of V_{ax} that correlated strongly against histology and diffusion MRI data with reduced errors upon protocol optimization, which testify to the applicability of this technique in clinical trials of TPNI.

Limitations. Unlike white matter in the CNS, biased V_{ax} and/or D_{ax} estimates may result from the violation of certain SMT model assumptions, i.e. large peripheral axon diameters ($\lesssim 20$ μm) and heterogeneous compartmental T_2s.

Future Directions. Random thermal noise will be introduced to the simulated data as a source of bias and will be fitted with SMT 10^4 times over 24 gradient directions to gauge the accuracy and precision of SMT-derived parameters.

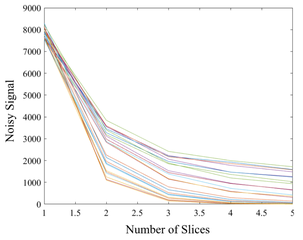

SNR = 30	V_{ax}	D_{ax} (μm^2/ms)
Histology	0.202	-
Noise-free	0.217	1.731
Rician noise$_1$	0.213	1.687
Rician noise$_2$	0.209	1.697
⋮		
Rician noise$_n$	$(V_{ax})_n$	$(D_{ax})_n$

Figure 7. The noise regime of the simulated noise-free signals will adhere to a Rician distribution.

ACKNOWLEDGEMENTS & REFERENCES

This work was supported by NIH grant R61NS127268 and the Barrow Neurological Foundation. KC thank TK and RDD for their dedicated mentorship and stimulating discussion throughout the course of this work.

1. Xu, S., Ito, A. (2023). *Current Opinion in Biomedical Engineering*, 100515.
2. Kaden, E., Kelm, N. D., Carson, R. P., Does, M. D., Alexander, D. C. (2016). *NeuroImage*, 139, 346-359.
3. Devan, S. P., Jiang, X., Bagnato, F., Xu, J. (2020). *Magnetic Resonance Imaging*, 74, 56-63.
4. Yablonskiy, D. A., Sukstanskii, A. L. (2010). *NMR in Biomedicine*, 23(7), 661-681.